Supplementary Material

Supplementary Table

Supplementary Table 1. Annual C budget for the growing and stagnant periods in the macroalgal habitat

Year	Period	Month	nC_T change (g C m^{-2} mon^{-1})	Air-sea C flux (g C m^{-2} mon^{-1})	C_T^{bio} uptake (g C m^{-2} mon^{-1})	Annual C_T^{bio} uptake (g C m^{-2} yr^{-1})
2020 –2021	Growing (cooling)	9–5	-1.4 (-2.8)	3.0	4.4 (5.8)	35.0 (47.7)
	Stagnant (warming)	6–8	2.1	0.6	-1.5	

Note. Data for 2021 were included to estimate the annual net changes of C_T^{bio}. The numbers in brackets were corrected for the effects of off-shore water intrusion.

Supplementary Texts

Supplementary Text 1

Details for measuring equipment

The continuous measurements of pCO_2 were performed with an autonomous pCO_2 monitoring system (Battelle, USA). The system was calibrated against certified reference CO_2 gas standards (280.20, 382.87, and 469.46 μatm pCO_2) provided by Scott-Marrin Inc (United States). For the accuracy test of the system, the measured xCO_2 value of the equilibrator headspace was compared with that of analytical gas streams delivered from the equilibrator to the detector (LICOR 7000) of the underway system. The intercomparison *via* reference samples in the pCO_2 range of 268.8, 318.3, 360.4, 435.2, and 620.4 ppm showed a highly linear ($r^2 > 0.0998$) correlation, and average deviations between regression-predicted and actual concentrations were < 2.5 μatm.

In situ pH were measured using an ion-selective field-effect transistor for pH (SeaFET™, United States) with the accuracy and precision of ±0.05 and 0.004 pH units, respectively. Temperature and salinity were measured using a MicroCAT CTD sensor (SBE37, United States). The sensor for temperature and conductivity was factory calibrated by Sea-Bird with reported precisions of ±0.002°C and ±0.003 mS cm^{-1}, respectively. All sensors were manually cleaned every week to avoid the effects of biofouling.

For the discrete measurements, the samples of seawater carbonate parameters (pH, A_T, and C_T) were collected *via* a Niskin sampler at 0.5 m below the surface and then transferred into 500 mL of a high-quality borosilicate glass container designed to minimize gas exchange with the atmosphere. The samples were poisoned with a mercuric chloride solution at the time of sampling and sealed with grease. pH was measured spectrophotometrically using m-cresol purple at 25°C (Clayton and Byrne 1993; Lee et al. 1996). Concentrations of A_T and C_T were determined using potentiometric and coulometric titration (VINDTA, Germany), respectively. The accuracy and precision of A_T and C_T (±1.6 μmol kg^{-1} for A_T; ±1.9 μmol kg^{-1} for C_T) were evaluated by titrating certified reference materials provided by A. Dickson (Scripps Institution of Oceanography, United States). Any discrepancies observed between measurements and certified values for the reference materials were applied to the measured values for samples analyzed during the same period in which the reference materials were analyzed. Samples for nutrient (HPO_4^{2-} and $Si(OH)_4$) were analyzed using a flow injection analyzer (QuAAtro, Germany) (Zhang et al. 2001).

Measurements of dissolved oxygen (DO) and dissolved organic carbon (DOC)

The measurement of DO was performed with a HOBO datalogger (Onset, United Sates) with ±0.2 mg L^{-1} accuracy. The cap of the sensor was replaced every six months to obtain reliable results. For DOC analysis, seawater sample was filtered through a pre-combusted GF/F 0.7 μm filter. The filtered seawater sample was immediately frozen and stored at –20°C after collection. During the measurement, each sample was acidified with 10% H_3PO_4 solution and purged with ultrapure O_2 gas to remove dissolved inorganic carbon (C_T). The C_T-free subsample was then injected into the total organic carbon analyzer (Shimadzu, Japan) and the oxidized DOC to CO_2 was measured using an infrared detector. The accuracy and precision were evaluated by measuring certified reference materials (Deep seawater reference: 41–45 μM; Low carbon water: ~1 μM) provided by D. Hansell (University of Miami, United States).

Supplementary Text 2

Effects of off-shore water intrusion on the carbonate dynamics of macroalgal habitat

The dynamics of the carbonate parameters in the study site are affected by off-shore water intrusion. Depending on the C level of the off-shore water, the contribution of biological activity to the carbonate dynamics is being either underestimated or overestimated. In our study, we made an estimation of the intrusion impact under several assumptions (see below).

A. Seasonal changes of C_T in off-shore water

For 2019–2020, seasonal variations in C_T were measured in February, April, August, and October at the off-shore water sampling sites along with the collinear latitude (36.08°N) of the study site (Figure 1A and Supplementary Figure 3A). The seasonal variations of off-shore nC_T concentrations were estimated by using the interpolated C_T ratios of the off-shore water to the study area (Supplementary Figures 3B, C). The resulting nC_T concentrations were slightly higher (< 1%) than the in-shore concentrations during the cooling months (January–May).

B. Residence time of seawater

Given the annual mean current velocity of the study site facing north, was 0.004 m s^{-1} (The Korea Operational Oceanographic System; Park et al. 2015) and the water depth is ~10 m, the residence time (RT) of seawater in the algal habitat was calculated using Equation (1):

$$\text{RT (d)} = \text{Water volume of the site (m}^3\text{)} / \text{Volume transported (m}^3\ \text{s}^{-1}\text{)} \tag{1}$$

where the Volume of water transported = Width of the section of outflow (m) · Depth (m) · Current velocity (m s^{-1}). Here, we assumed that a) there was no water flow east-west direction, and b) the water was discharged from the site through a small channel due to a rocky island located in the course of outflow. Depending on the actual water volume of the study site (~5.0×10^6 m^3) and the width of the outflow section (~200 m)—which were not directly measured in this study—the estimated residence time (~10 days) could be highly variable.

C. Effects of off-shore water intrusion

The net C_T uptake by biology (C_T^{bio}) corrected for the off-shore water intrusion was computed for the growing period (September–May) according to the equations below:

$$nC_T^{meas} = nC_T^{corr} \times df + nC_T^{off\text{-}shore} \times (1 - df) \tag{2}$$

where df is the dilution factor of the off-shore water (= $1/(1+\alpha)$, where α is the data interval (30 days) divided by the RT), and the values of nC_T^{meas} and nC_T^{corr} are both for the study site (in-shore water).

$$C_T^{bio} = -\text{the rate of } nC_T^{corr} \text{ changes} \times \text{time} + \Sigma\text{C changes } \textit{via} \text{ flux}^{air\text{–}sea} \tag{3}$$

The changes in nC_T^{corr} during the growing period with the residence time of 10 days were –22.5 μmol C_T kg^{-1} mon^{-1} (Supplementary Figure 3D). The change of slope resulted in ~30% enhancement of the C_T^{bio} during the growing period.

Supplementary Text 3

Temperature dependence of thermodynamic equilibrium constants

The carbonate chemistry of seawater is essentially determined by a few components of seawater: CO_2, HCO_3^-, CO_3^{2-}, OH^- and H^+. Although the concentrations of individual species cannot be directly measured, four parameters—pCO_2, pH, A_T (= $[HCO_3^-] + 2[CO_3^{2-}] + [B(OH)_4^-] + [OH^-] - [H^+]$ – minor components) and C_T (= $[CO_2] + [HCO_3^-] + [CO_3^{2-}]$)—can be determined and used together to describe the carbonate dynamics in seawater. Also, Ω_{arag} (the degree of aragonite saturation state defined as a ratio of the ionic product, $[Ca^{2+}]\,[CO_3^{2-}]$, to its theoretically saturated value at a given condition) serves as a proxy for the potential dissolution of biogenic minerals in response to ocean acidification. When more than two of the carbonate parameters (i.e. C_T and A_T) have been measured on a single seawater sample, it is possible to compute the other dependent parameters by using mass-conservation equations and equilibrium constants.

A temperature change thermodynamically leads to a change in standard free energy for reactions representing the marine carbonate system and, thus, in the thermodynamic equilibrium constants. The equilibrium constants for the processes below (Equations 1-3) are empirically given by the listed expressions (Equations 5-7), which are dependent on temperature changes.

$$CO_2\,(g) \overset{K0}{\leftrightarrow} CO_2\,(aq) \qquad K_0 = [CO_2\,(aq)] \,/\, fCO_2 \qquad (1)$$

$$CO_2\,(aq) + H_2O \overset{K1}{\leftrightarrow} H^+ + HCO_3^- \qquad K_1 = [H^+]\,[HCO_3^-] \,/\, [CO_2\,(aq)] \qquad (2)$$

$$HCO_3^- \overset{K2}{\leftrightarrow} H^+ + CO_3^{2-} \qquad K_2 = [H^+]\,[CO_3^{2-}] \,/\, [HCO_3^-] \qquad (3)$$

$$\text{Overall reaction: } CO_2\,(aq) + H_2O + CO_3^{2-} \xleftrightarrow{K1/K2} 2HCO_3^- \qquad (4)$$

$$\mathrm{Ln}(K_0) = 93.4517(100/T) - 60.2409 + 23.3585\,\mathrm{Ln}(T/100)$$
$$+\, S[0.023517 - 0.023656\,(T/100) + 0.0047036\,(T/100)^2] \quad \text{(Weiss 1974)} \quad (5)$$

$$\mathrm{Log}_{10}(K_1) = -3633.86/T + 61.2172 - 9.67770\,\mathrm{Ln}(T)$$
$$+\, 0.011555S - 0.0001152S^2 \quad \text{(Lueker et al. 2000)} \quad (6)$$

$$\mathrm{Log}_{10}(K_2) = -471.78 - 25.9290 + 3.16967\,\mathrm{Ln}(T)$$
$$+\, 0.01781S - 0.0001122S^2 \quad \text{(Lueker et al. 2000)} \quad (7)$$

where fCO_2, T, and S are the fugacity of CO_2 in pure CO_2 gas or in air (unit: atm), temperature (K) and salinity, respectively. Temperature dependence of K_0, K_1, K_2 (mol kg^{-1}), and K_1/K_2 in the range of temperature, 10–25°C, are illustrated in Supplementary Figures 4A–C. Shifts in the *pK* values of the first and second dissociation constants of carbonic acid (Equations 6 and 7) lead to changes in the proportions of carbonate species.

Temperature-induced changes in the concentrations of carbonate species

Under given conditions of C_T and A_T, the expression for A_T (= $[HCO_3^-] + 2[CO_3^{2-}] + [B(OH)_4^-] + [OH^-] - [H^+]$ – minor components) can be rewritten in terms of C_T and H^+ (Dickson et al. 2007) because most of the individual species in the simplified definition of A_T can be related to a combined equilibrium mass-balance expression which involves suitably-defined equilibrium constants, pH scale (total scale), and the total stoichiometric concentration of the species.

Equations (2) and (3) are rearranged and substituted into the definition of C_T (= $[CO_2] + [HCO_3^-] + [CO_3^{2-}]$) to give

$$C_T = [CO_2(aq)]\left(1 + \frac{K_1}{[H^+]} + \frac{K_1K_2}{[H^+]^2}\right) \tag{8}$$

Thus

$$[CO_2(aq)] = \frac{C_T}{[H^+]^2 + K_1[H^+] + K_1K_2} \times \mathbf{[H^+]^2} \tag{9}$$

$$[HCO_3^-] = \frac{C_T}{[H^+]^2 + K_1[H^+] + K_1K_2} \times \boldsymbol{K_1[H^+]} \tag{10}$$

$$[CO_3^{2-}] = \frac{C_T}{[H^+]^2 + K_1[H^+] + K_1K_2} \times \boldsymbol{K_1K_2} \tag{11}$$

For borate ion and hydroxide concentrations,

$$[B(OH)_4^-] = \frac{B_T}{1 + [H^+]/K_B} \tag{12}$$

$$[OH^-] = \frac{K_w}{[H^+]} \tag{13}$$

where B_T, K_B, and K_w are the total concentrations of boron (= $[B(OH)_3] + [SO_4^-]$), the dissociation constants for boric acids and water, respectively (Dickson et al. 2007). The combination of the expression for A_T with the equilibrium expressions for each species (9–13) can be solved for $[H^+]$. Once $[H^+]$ has been calculated, the concentrations of C species relevant to pCO_2, pH, and Ω_{arag} can be all determined.

As temperature increases, the value of K_0 decreases (Supplementary Figure 4A), whereas the values of K_1 and K_2 increase at different rates (Supplementary Figure 4B). Such disproportional increases in K_1 and K_2 eventually lead to a decrease in the K_1/K_2 ratio with increasing temperature (also increasing with increasing proton concentration; Supplementary Figure 4C). The resulting decrease in the K_1/K_2 ratio leads to a decrease in the concentration of HCO_3^- but concurrently to increases in the concentrations of CO_2 (*aq*) and CO_3^{2-} (Eq. 4), as elaborated in details elsewhere (Cai et al. 2020; Zeebe and Wolf-Gladrow 2001).

Temperature-induced changes in the values of carbonate parameters

In response to a change in seawater temperature, the overall changes in the equilibrium constants and the concentrations of carbonate components lead to a significant increase and decrease in pCO_2 (Figure 3A and Supplementary Figure 4D) and pH (Figure 3B and Supplementary Figure 4E), respectively. Theoretical rates of change for these parameters are known to be 4% pCO_2 increase $^{o}C^{-1}$ and 0.017 pH decrease $^{o}C^{-1}$ (Lee and Millero 1995; Takahashi et al. 2002), respectively. On the contrary, because both C_T and A_T are temperature independent the resulting values of these parameters do not change with varying temperatures under abiotic conditions. Ω_{arag}—the carbonate parameter directly proportional to $[CO_3^{2-}]$—shows a subtle increase in response to increasing temperature (Figure 3D and Supplementary Figure 4F). The low sensitivity of Ω_{arag} to temperature can be inferred from Equations (9-11) (in bold text) in that $[CO_3^{2-}]$ is less affected by rapidly changing $[H^+]$ than the other carbonate species.

Dynamics of carbonate parameters in the macroalgal habitat: sensitivities of Ω_{arag} to perturbations

In response to temperature changes over seasons, pCO_2 and pH are highly sensitive to temperature variation. By comparison, variations of Ω_{arag} are considerably smaller than those of pCO_2 (and pH) because they are dominantly controlled by nonthermal factors in the highly productive habitats. The variations of Ω_{arag} are more sensitive to variations of C_T and A_T (in particular, the C_T-to-A_T ratio). The C_T/A_T ratio is a good measure of the carbonate ion concentration in the pool of C_T: a lower ratio means a higher proportion of carbonate ions. In some cases, changes in Ω_{arag} can be more strongly influenced by the consumption of carbonate ions by phytoplankton than temperature change. Regarding different sensitivities of carbonate parameters (other than pCO_2 and pH) to gas equilibrium and biological activities among regions, Cai et al. (2020) proposed that the impacts of local modifications and the timescale (compared with that of equilibration) determine the first-order mechanism of control. In our macroalgal habitat, where the magnitude of C disequilibrium is large and the main processes (primary production and respiration) that contribute to the carbonate chemistry act much faster than the timescales of equilibrium, the dynamics of Ω_{arag} are mostly dictated by biology. Our finding is similar to the trends observed in the Pacific coasts under the strong influence of upwelling and biological CO_2 removal (with a short timescale) (Cai et al. 2020).

Supplementary Figures

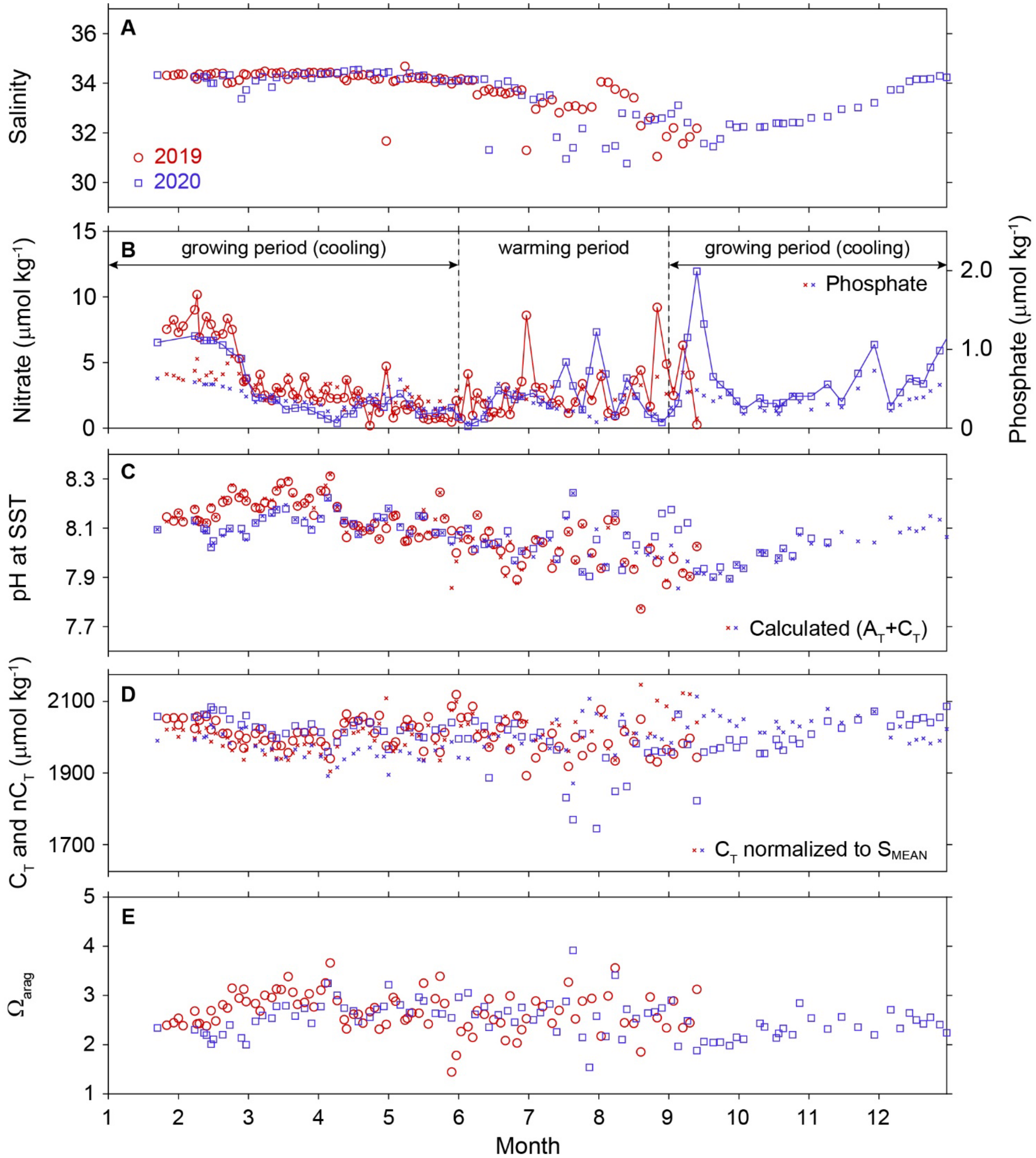

Supplementary Figure 1. (A) Salinity, **(B)** nitrate and phosphate concentrations **(C)** pH, **(D)** C_T and nC_T, and **(E)** Ω_{arag} for the period 2019 (red)–2020 (blue) during the discrete measurements. Note that the episodic decrease in C_T observed during the summer months was due to a sudden decrease in salinity caused by a typhoon.

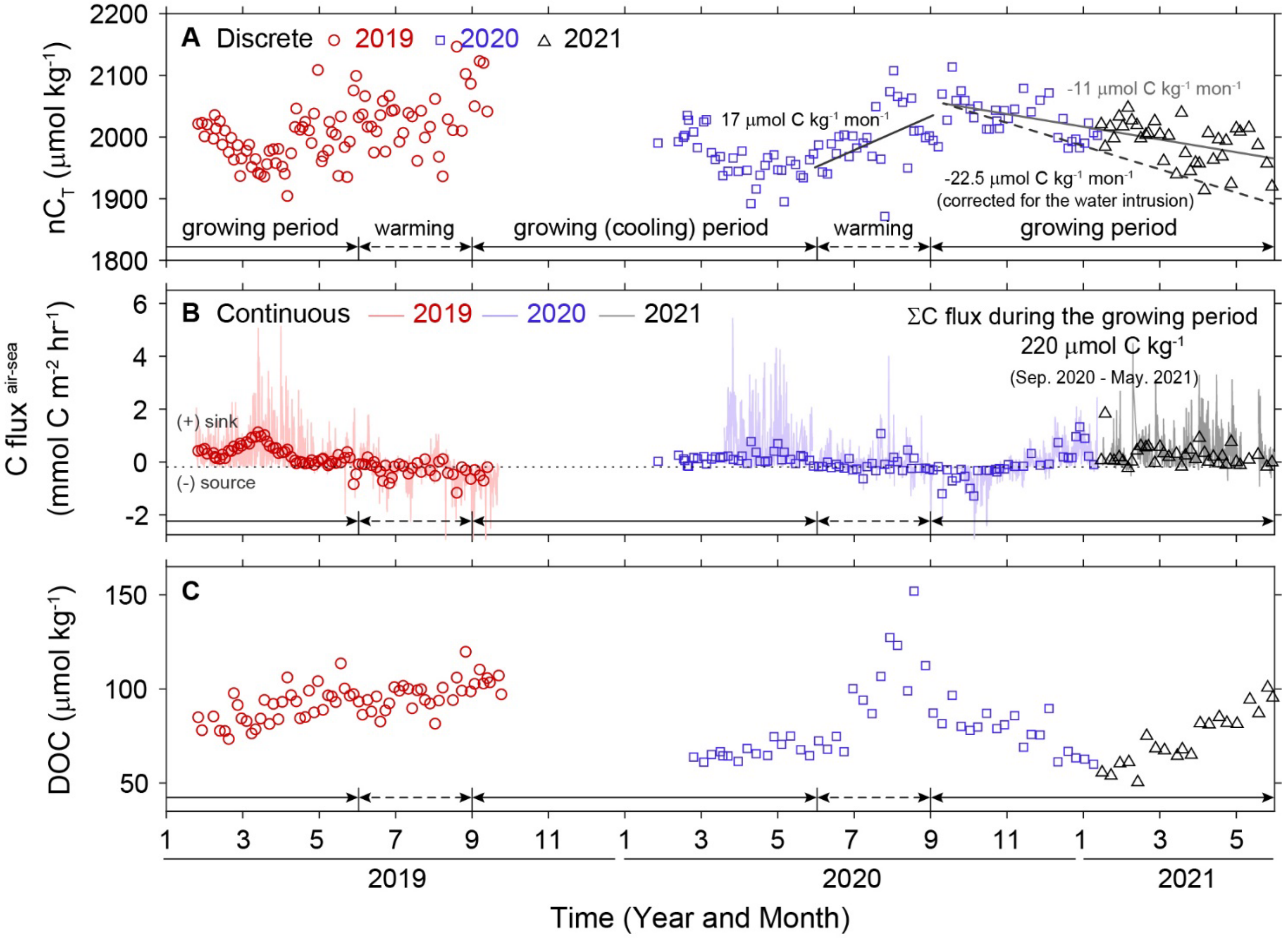

Supplementary Figure 2. **(A)** Discrete nC_T, **(B)** discrete and continuous air-sea C flux, and **(C)** discrete dissolved organic C (DOC) concentrations for the period 2019–2021 (2019: red; 2020: blue; 2021: black). Solid and dotted arrows indicate the growing period (September–May) and the stagnant growth period (June–August). Data for 2021 were included to estimate the annual net changes of C_T^{bio}.

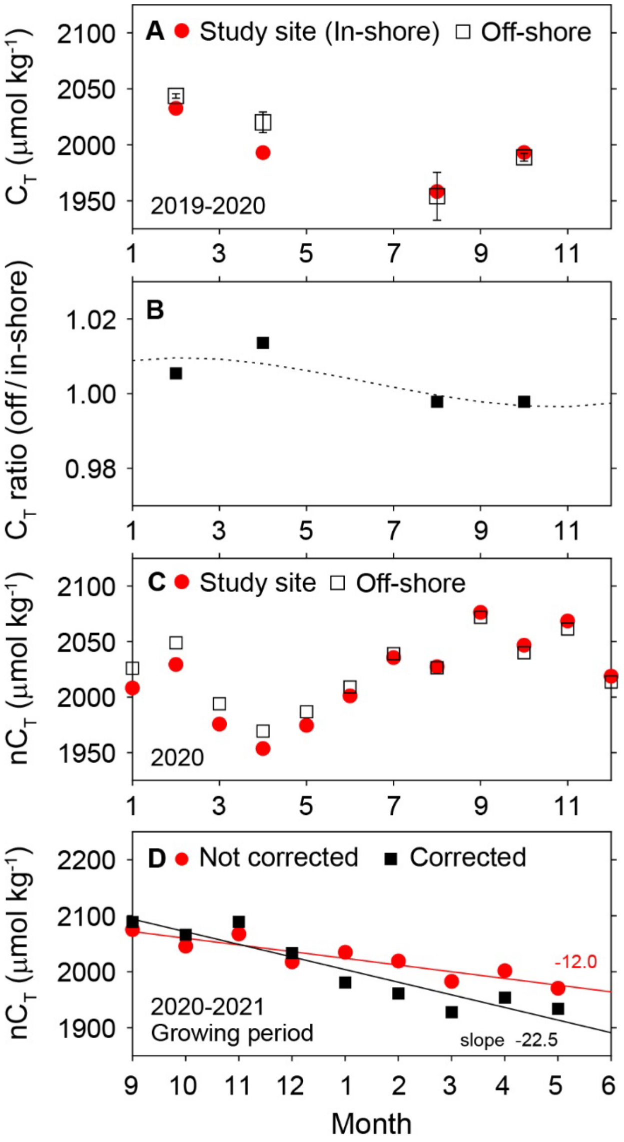

Supplementary Figure 3. (A) Seasonal variations of C_T in the off-shore water and the study site for the period 2019–2020, **(B)** the ratios of C_T between the off-shore and in-shore water (fit: $y = ax^3 + bx^2 + cx + d$; $a = 4.2 \times 10^{-5}$, $b = -8.1 \times 10^{-4}$, $c = 0.0029$, and $d = 1.0067$), **(C)** the monthly mean nC_T dynamics in the study site in 2020 and the estimated changes of nC_T in the off-shore water (the mean salinity values of the two regions were equal to 33.4), and **(D)** the changes in nC_T during the growing period (September–May 2020–2021) without and with the correction of the effects of off-shore water intrusion.

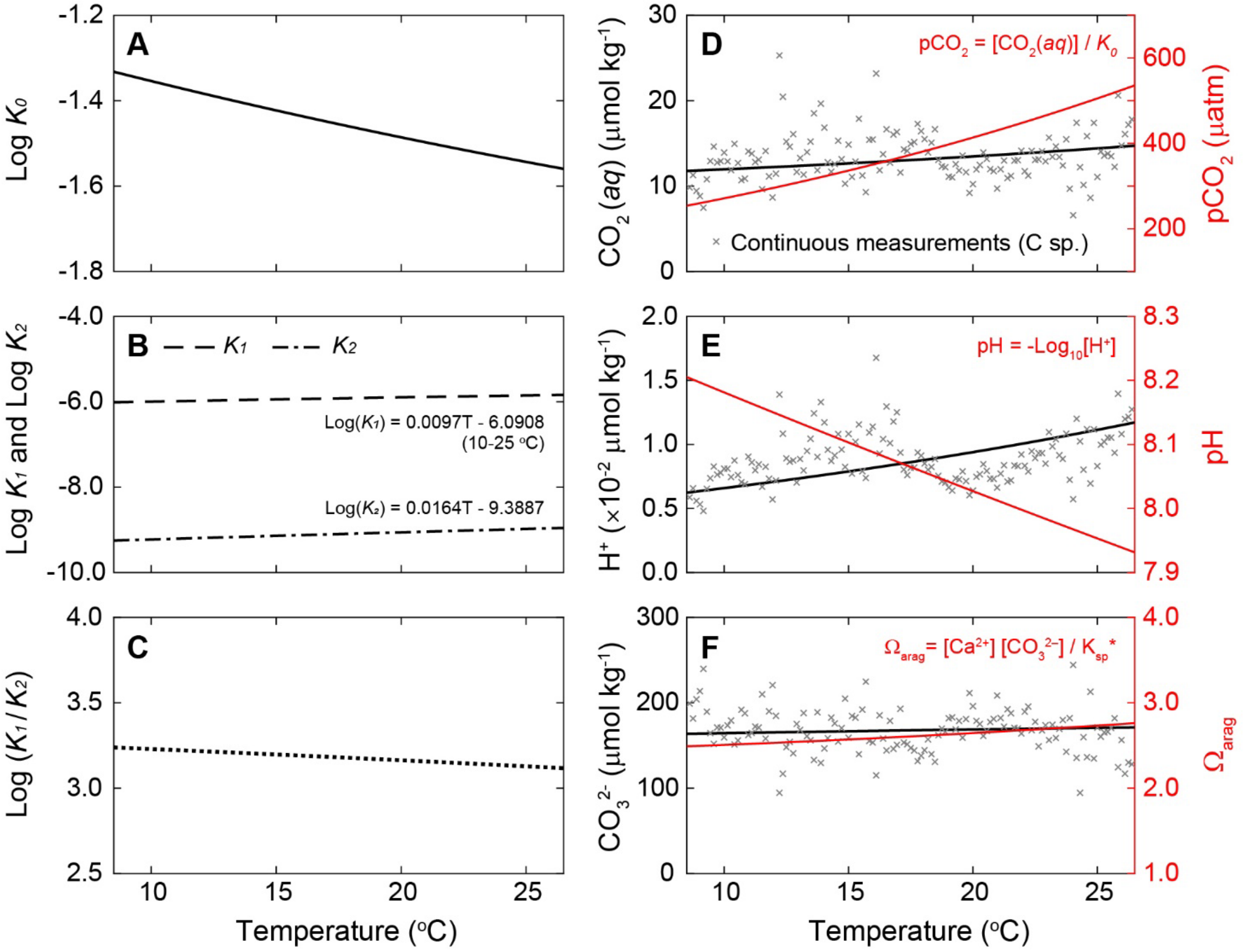

Supplementary Figure 4. (A-C) Temperature dependence of thermodynamic constants in the closed system: **(A)** K_0, **(B)** K_1 and K_2, and **(C)** K_1/K_2 (expressed on a log scale). Changes are calculated at the constant values of C_T (2001.9 µmol kg^{-1}), A_T (2239.2 µmol kg^{-1}) and salinity (33.5), which were the mean concentrations during the discrete measurements. **(D-F)** Effects of temperature on the concentrations of key carbonate species (black lines) and the values of carbonate parameters (red lines): **(D)** CO_2 (aq) and pCO_2, **(E)** H^+ and pH, and **(F)** CO_3^{2-} and Ω_{arag} (K_{sp}^* is the stoichiometric solubility product). Crosses (in grey) represent the concentrations of carbonate species measured during the discrete measurements (2019–2020).

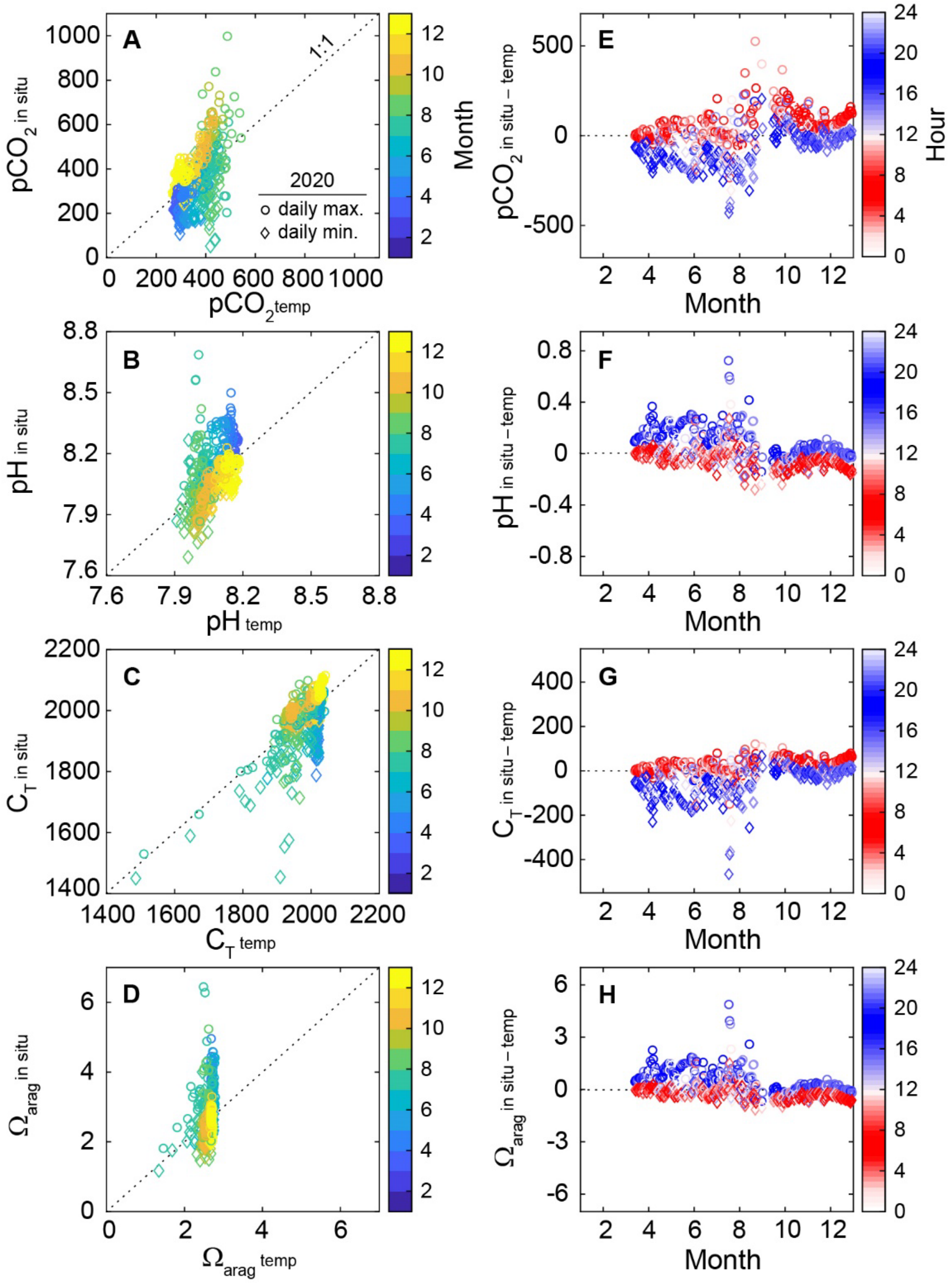

Supplementary Figure 5. (A-D) Relationship between the *in situ* carbonate parameters ($C_{in\ situ}$) obtained during the continuous measurements in 2020 and the parameters resulted from the change of temperature in the closed system (C_{temp}). Only the daily extremes (circles: maximum; diamonds: minimum) are displayed with being color-coded by month. **(E-H)** The daily extreme values of the differences between $C_{in\ situ}$ and C_{temp}. The color of the symbols overlaid by the time of measurement.

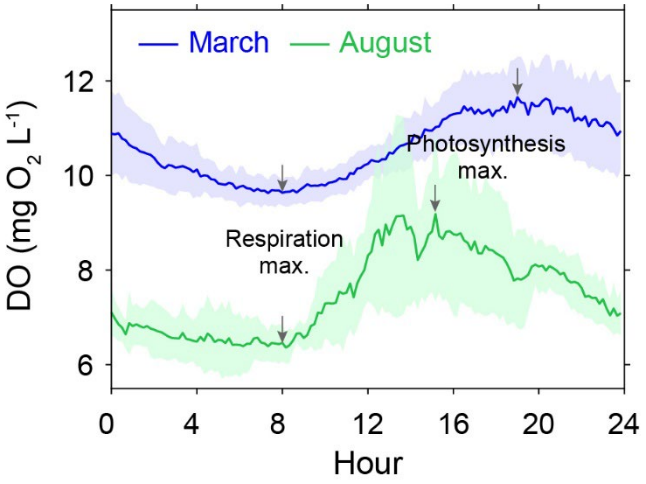

Supplementary Figure 6. Diurnal changes in dissolved oxygen (DO) concentration in a cooling period (March) and a warming period (August) in the study site. The arrows indicate the time at which the minimum and the maximum levels of DO were observed during a day (Photosynthesis increases DO and pH but decreases pCO_2 and C_T; respiration, *vice versa*).

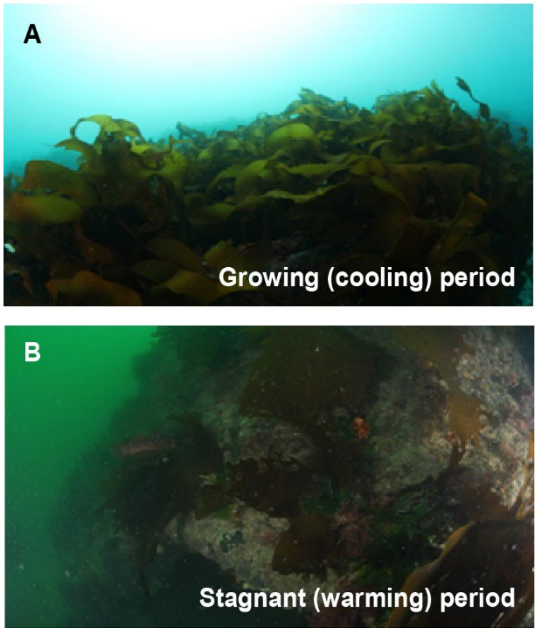

Supplementary Figure 7. Photos of the macroalgal habitat during **(A)** the growing (photosynthesis dominant) period and **(B)** the stagnant (respiration active) period.